Scripta Materialia 156 (2018) 129–133

Contents lists available at ScienceDirect

Scripta Materialia

journal homepage: www.elsevier.com/locate/scriptamat

Regular article

Activation energy for plastic flow in nanocrystalline CoCrFeMnNi high-entropy alloy: A high temperature nanoindentation study

Dong-Hyun Lee [a,1], In-Chul Choi [b,1], Guanghui Yang [a], Zhaoping Lu [c], Megumi Kawasaki [d], Upadrasta Ramamurty [e], Ruth Schwaiger [b,*], Jae-il Jang [a,*]

[a] Division of Materials Science and Engineering, Hanyang University, Seoul 04763, Republic of Korea
[b] Institute for Applied Materials, Karlsruhe Institute of Technology, Karlsruhe 76344, Germany
[c] State Key Laboratory for Advance Metals and Materials, University of Science and Technology Beijing, Beijing 10083, People's Republic of China
[d] School of Mechanical, Industrial & Manufacturing Engineering, Oregon State University, Corvallis, OR 97331, USA
[e] School of Mechanical and Aerospace Engineering, Nanyang Technological University, Singapore 639798

ARTICLE INFO

Article history:
Received 1 June 2018
Received in revised form 9 July 2018
Accepted 10 July 2018
Available online 25 July 2018

Keywords:
High-entropy alloy
Nanoindentation
Activation energy barrier
Nanocrystalline metal

ABSTRACT

Nanoindentation experiments in the temperature (T) range of 298 and 573 K were performed to determine the activation energy (Q) for the plastic flow in a nanocrystalline CoCrFeMnNi high-entropy alloy, which was synthesized using high-pressure torsion. A marked increase in Q from ~0.5 to ~1.8 eV was observed when T is increased from 473 to 523 K, which correspond to ~0.3 and ~0.34 T_m (T_m: melting temperature), respectively. Detailed analysis reveals that this transition is associated with the additional activation of the grain boundary diffusion mechanism in enhancing plasticity.

High-entropy alloys (HEAs) or compositionally complex alloys (CCAs), which are multicomponent alloys containing five or more elements in (near-)equal atomic percent, have attracted significant research interest over the past decade due to their simple microstructures with interesting mechanical properties [1–4]. Recently, it has been reported that the mechanical performance of HEAs can be further enhanced by reducing the grain size, d, to the nanocrystalline (nc) regime with $d < 100$ nm [5–7]). One of the ways to obtain a nc HEA is through the high-pressure torsion (HPT) process; it was reported that d of CrMnCoFeNi HEA can be reduced from ~40 μm to ~40 nm [8–11] via HPT. The mechanical behavior of such nc HEAs is also reasonably well understood [8–12]; this was mostly accomplished by employing small-volume mechanical testing techniques such as nanoindentation and micro-pillar compression [10–13] due to the limited volume of target material available. In addition to hardness H and reduced modulus E_r, parameters such as the strain-rate sensitivity m and activation volume V^*, which are essential for developing an understanding of the deformation mechanism, can be extracted via nanoindentation [10, 14, 15]. However, most of these studies are confined to room temperature (RT). To the best of our knowledge, there is only one paper dealing with high-temperature nanoindentation of nc HEA, in which Maier-Kiener et al. [16] reported m and V^* of a nc HEA. For a complete understanding of a material's thermally-activated plastic deformation process, a good estimate of the activation energy Q for such flow, is also essential. Keeping this in view, we performed high-temperature nanoindentation experiments on a nc CrMnCoFeNi HEA processed by HPT so as to estimate Q at various temperatures, T. The operating deformation mechanisms are interpreted on the basis of the data obtained.

The CoCrFeMnNi HEA (20 at.% for each element) used in this study was prepared by arc-melting a mixture of pure metals (purity >99 wt %) in a Ti-gettered high-purity Ar atmosphere. Disks of 10 mm diameter and ~0.8 mm thickness were machined for the HPT process, which was conducted at RT under an applied pressure of 6.0 GPa for a total of 2 turns using a rotational speed of 1 rpm. In the as-cast alloy, d is ~40 μm. Hence, it referred to as coarse-grained (cg) HEA hereafter. Upon HPT, d reduces to ~38 nm [10, 11]. The surfaces of cg and nc specimens were first mechanically polished with fine SiC paper (grit number up to 2000) and then electro-polished at 58 V for 20 s in a mixture of 90% acetic and 10% perchloric acid at RT.

The nanoindentation experiments were performed using the Nanoindenter G200 XP (Keysight Technologies, Santa Rosa, CA, USA) operated with the continuous stiffness measurement (CSM) mode at six different T of 298 (RT), 373, 423, 473, 523, and 573 K. A laser heating stage (Surface Tec., Hückelhoven, Germany) and a Berkovich indenter made of sapphire were utilized for the high T experiments. Both the

* Corresponding authors.
E-mail addresses: ruth.schwaiger@kit.edu (R. Schwaiger), jijang@hanyang.ac.kr (J. Jang).
[1] Equally contributing authors (D.-H. Lee and I.-C. Choi).

https://doi.org/10.1016/j.scriptamat.2018.07.014
1359-6462/

tip and sample were independently heated by laser via an optical fiber; details of this setup can be found in Refs. [17, 18]. This arrangement not only minimizes the thermal drift (to <0.1 nm/s), but also allows for stabilization of the contact temperature, guaranteeing, thus, a well-defined homogeneous temperature distribution. The correction of the frame stiffness and the calibration for tip area function were performed according to the procedure outlined by Oliver and Pharr [19]. More than 10 tests were conducted for each of the testing conditions.

For evaluating the T-dependence of H, nanoindentation tests were performed at a constant indentation strain rate, $\dot{\varepsilon}_i = h^{-1}(\mathrm{d}h/\mathrm{d}t)$, where h is the indentation depth and t is time; the specimens were loaded to maximum indentation depth h_{max} of 1700 nm at a constant $\dot{\varepsilon}_i$ of 0.025 s^{-1}. In order to evaluate m and V^*, the indentation strain-rate jump (SRJ) tests were carried out. During these, the sample experiences three different $\dot{\varepsilon}_i$ (of 0.025, 0.008, and 0.0025 s^{-1}) until h_{max} is reached, as depicted in Fig. S1(a) of Supplementary material. The indentation impressions were imaged using atomic force microscopy (AFM), XE-100 (Park System, Suwon, Korea).

Possible changes in the microstructure of the high T tested HEA were investigated using transmission electron microscopy (TEM; JEM 2100F, JEOL Ltd., Tokyo, Japan). For TEM specimen preparation, focused ion beam (FIB) milling using a SCIOS (FEI Co., Hillsboro, OR) was utilized. During TEM analysis, element mapping was performed using energy dispersive X-ray spectroscopy (EDS).

Fig. 1a shows representative load-displacement (P-h) responses obtained on cg and nc HEAs at a variety of T. With increasing T, the load at the maximum displacement P_{max} decreases from ~130 mN at 298 K to ~100 mN at 573 K for cg HEA, while it changes from ~320 to ~220 mN for nc HEA. The H was determined from CSM [19]; the variations of H with $1/T$ are displayed in Fig. 1b. As expected, (i) H of nc HEA is much higher than that of cg HEA at all T, which is due to the grain refinement [9–11], and (ii) H decreases with increasing T in both cases. The T-dependence of plastic flow resistance (represented by H here) of polycrystalline metals and alloys can generally be described by the equation: $H = A \exp(B/T)$, where A and B are material constants; B is often referred to as softening coefficient [14, 20]. While this equation describes the cg HEA's response within the entire T range examined, a bilinear response in $\ln(H)$ vs. $1/T$ plot of nc HEA can be noted, with a significant change in the slope occurring at ~473 K. Since the value of $\partial(\ln H)/\partial(1/T)$ is closely related to (although not exactly the same as) Q [14, 20], the change in slope observed in Fig. 1b indicates a change in the nature of deformation in nc HEA. This will be discussed later.

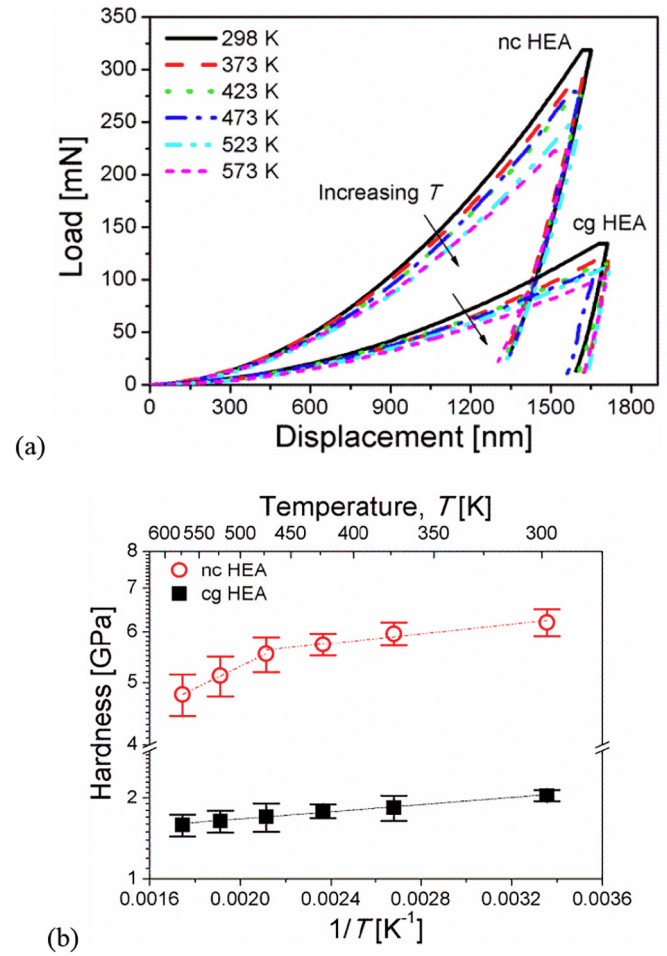

Fig. 1. Results of the nanoindentation experiments: (a) representative P-h responses obtained at different indentation strain rates for cg and nc HEAs and (b) the variation in the hardness as a function of $1/T$.

The material pile up characteristics around the indent can indicate the nature of the plastic deformation; pronounced pile-up is often observed in a material that does not strain harden considerably [21, 22]. The ratio of pile-up height $h_{pile\text{-}up}$ (measured with AFM) to residual displacement h_r (obtained from the P-h responses), $h_{pile\text{-}up}/h_r$, is plotted in Fig. 2 as a function of T. In cg HEA, a linear, but marginal, decrease in $h_{pile\text{-}up}/h_r$ with T is noted. This observation suggests that work hardening behavior of cg HEA is not affected in any significant manner by T. The nc HEA's response is significantly different. At 298 K, the pile-up is pronounced, which is possibly due to the lack of work hardening ability in this HEA [12, 14]. While $h_{pile\text{-}up}/h_r$ decreases with increasing T, the reduction accelerates for $T > 473$ K, indicating a strong change in the work hardening behavior.

The above changes in $\partial(\ln H)/\partial(1/T)$ and work hardening behavior at a T of ~473 K suggest a transition in the deformation mechanism of nc HEA. Before discussing that and to rule out the possibility of microstructural instability being the reason for the observed transition, the results of TEM analysis performed on the nc HEA sample that was tested at 573 K are presented (Fig. 3). The bright-field (BF) image exhibits a nc microstructure with d ~36 nm, which is consistent with the initial grain structure with d ~38 nm [10, 11]. Elemental mapping of the imaged area using EDS indicates homogeneous distributions of constituent elements, i.e., no obvious segregation or clustering can be seen. These

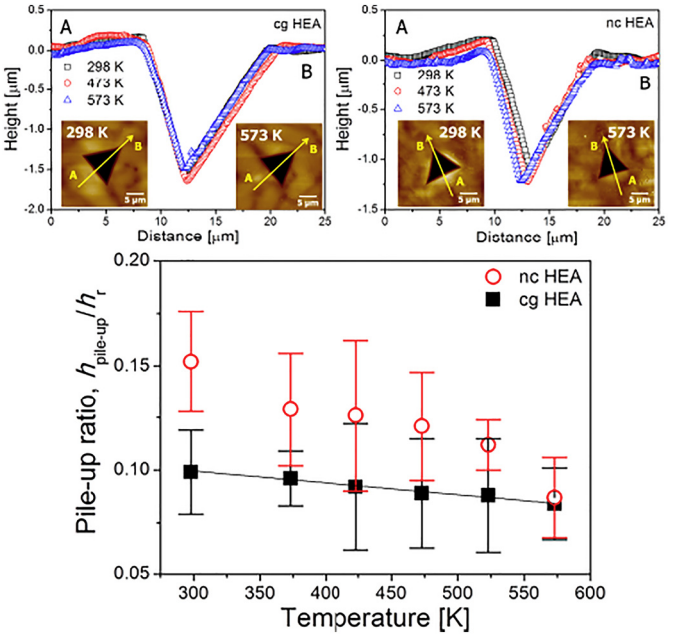

Fig. 2. Representative AFM data (for cg and nc HEAs) and the variations in pile-up ratio as a function of T.

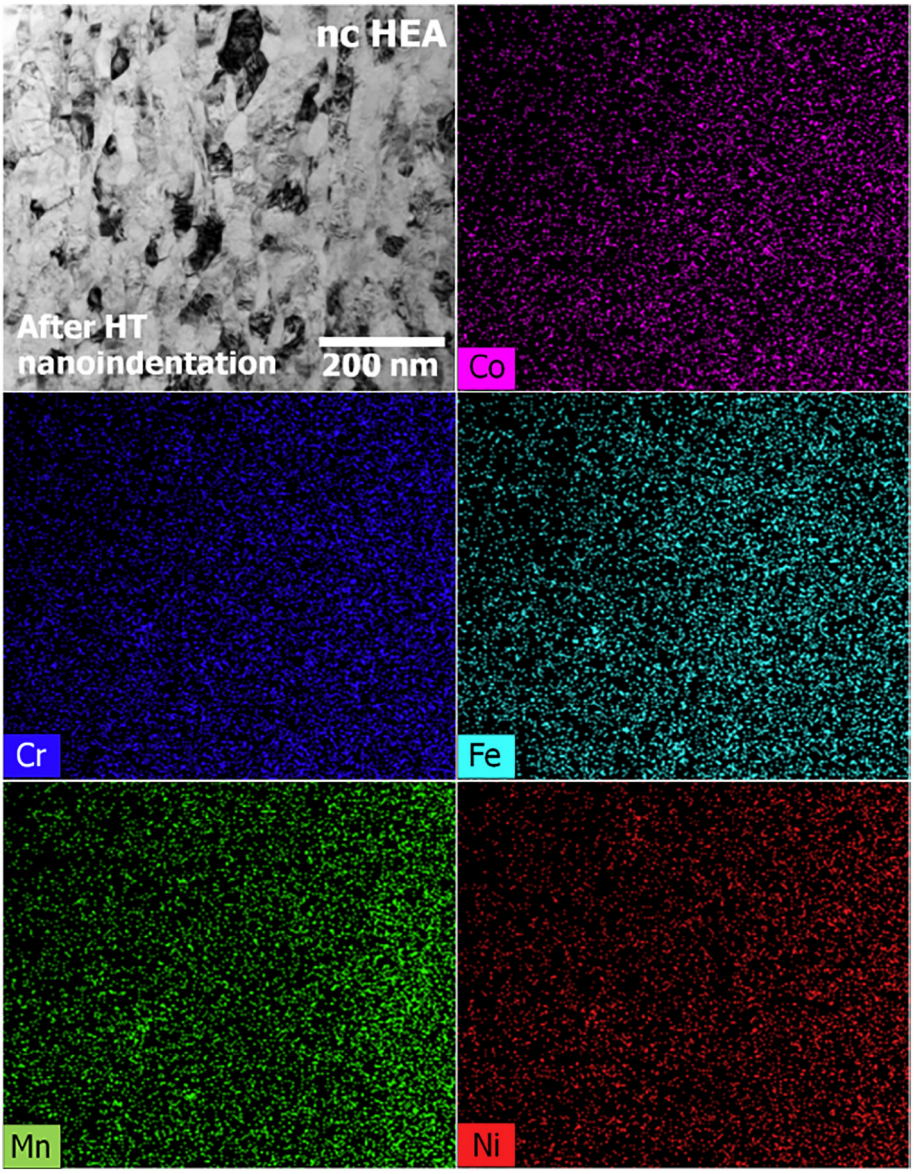

Fig. 3. Results of the TEM analysis: bright-field image and corresponding EDS maps of nc HEA which was subjected to nanoindentation at 573 K prior to TEM.

results lead us to conclude that the nc HEA is structurally stable within the T range examined.

To ascertain the dominant deformation mechanism(s) in nc HEA, a series of SRJ tests were performed on nc HEAs at various T in order to estimate $m = \partial(\ln H)/\partial(\ln \dot{\varepsilon}_i)_{\varepsilon,T}$ and $V^* = \sqrt{3}CkT(\partial \ln \dot{\varepsilon}_i/\partial H)$, where C is the constraint factor (~3) for fully-plastic deformation [23] and k is the Boltzmann constant. Representative P-h curves for nc HEAs obtained from SRJ tests were displayed in Fig. S1 of Supplementary material, in which the corresponding H-h curves are also shown. The variations in m and V^* as a function of T for nc HEAs are summarized in Fig. S2 of Supplementary material (the reason for placing these data in Supplementary material is that Maier-Kiener et al. [16] have reported such data for an nc HEA with the same composition). The value of m remains almost constant (~0.015) until 423 K and increases from 473 K onwards with T. In contrast, V^* has a peak at 423 K. These trends are in a good agreement with the data reported by Maier-Kiener et al. [16], while a slight difference in the absolute values can be noted. Although these results do indicate a possible change in the deformation mechanism, they are insufficient to confirm a mechanistic transition whereas, Q, being a thermodynamic parameter for the thermally-activated plastic flow can provide such confirmation.

Generally, in the Arrhenius-type constitutive law for T-dependent plastic strain rate, $\dot{\varepsilon} = \dot{\varepsilon}_0 \exp(-Q/kT)$, where $\dot{\varepsilon}_0$ is a pre-exponential constant, the barrier Q is described as the stress-dependent Gibbs free energy ΔG for the activation of flow. While ΔG is given as $\Delta H - T\Delta S$ (where ΔH and ΔS are activation enthalpy and entropy, respectively), ΔS for plastic flow tends to be very small and hence often ignored (e.g., 0.0004 eV/K for Cu with d ~18 μm [24]). Thus, for plastic deformation, ΔG is often assumed to be equal to ΔH [24, 25]. By applying the definition of $\Delta H = \Delta G - T(\partial \Delta G/\partial T)$ to Arrhenius-type equation, ΔH can be determined as [24–26]:

$$\Delta H = -kT^2 \frac{\partial \ln(\dot{\varepsilon}/\dot{\varepsilon}_0)}{\partial T} = -kT^2 \frac{\partial \ln \dot{\varepsilon}}{\partial H}\frac{\partial H}{\partial T} \tag{1}$$

and with $V^* = \sqrt{3}CkT(\partial \ln \dot{\varepsilon}/\partial H)$,

$$\Delta H = -T\frac{V^*}{\sqrt{3}C}\left(\frac{\partial H}{\partial T}\right) = -T\frac{V^*}{\sqrt{3}C}\left(-\frac{H}{T^2}\frac{\partial(\ln H)}{\partial(1/T)}\right) = \frac{HV^*}{\sqrt{3}CT}\cdot\frac{\partial(\ln H)}{\partial(1/T)} \tag{2}$$

Fig. 4 summarizes the T-dependence of the *apparent* activation enthalpy ΔH, estimated using Eq. (2), for nc HEA. For $T \leq 473$ K

(~0.3T_m), $\Delta\mathcal{H}$ is ~0.5 eV. This barrier can be re-cast as "normalized activation enthalpy" $\Delta\mathcal{H}/\mu b^3$ (where shear modulus μ and length of Burger's vector b are ~80 GPa [27] and ~0.25 nm [10], respectively, for this alloy) of ~0.06. This is much lower than those reported (0.2–1.0) for low-T dislocation plasticity that typically is controlled by the forest dislocation interactions [28]. Such a low activation barrier suggests that deformation is governed by grain boundary (GB)-mediated dislocation activities such as the emission of partial or perfect dislocations from GBs, for which the activation barrier is expected as 0.7–1 eV [26, 29–31]. Recently, Lin et al. [32] conducted in-situ high-resolution TEM analysis of GB dislocation activities in an HPT-processed nc CoCrFeMnNi HEA and reported that Frank partial dislocations at GBs were relaxed by emitting Shockley partials and the emitted partials glide into the grain under e-beam irradiation. Such an easy activation of the partial dislocation emission in nc HEA [32] agrees well with our measurements of low $\Delta\mathcal{H}$ and suggests that the plastic deformation in nc HEA below a T of 473 K may be primarily governed by such a mechanism.

From Fig. 4, a marked and sharp increase in $\Delta\mathcal{H}$ from ~0.5 to ~1.8 eV for T > 473 K can be noted. This relatively high $\Delta\mathcal{H}$ approaches that of GB diffusion of Ni in CoCrFeMnNi HEA, ~2.3 eV [33]. In addition, since T ~523 K corresponds to relatively high homologous temperature (~0.34 of T_m), it is reasonable to expect more pronounced GB diffusion. This can be related with a large volume of non-equilibrium GBs in HPT-processed nc HEA [9]; such GBs contain a high concentration of extrinsic dislocations giving a larger excess free energy, and hence exhibit enhanced diffusivities (or lower activation barrier) compared to typical GBs [34, 35]. For T > 473 K, the values of m (up to ~0.03) and V^* (~20b^3) (see Fig. S2) suggest that GB diffusion-related phenomena (such as Coble creep and GB sliding which are expected to show much higher m values and lower V^* values) may not be predominant, but they may still play some role in the plastic deformation. For instance, diffusive transport across GBs may promote GB-mediated dislocation activity such as dislocation nucleation, climb, and annihilation at GBs that often are aided by diffusion, GB sliding, and grain rotation [36, 37]. In this context, it is interesting to note that Maier-Kiener et al. [16] report a further increase in m (to 0.1) and a commensurate drop in V^* to <10b^3 at 673 K, indicative of an even more prominent role of GB diffusion at that T. On this basis, we can conclude that the hot deformation of nc HEA at T ≥473 K, can be enhanced by GB diffusion while still being governed by GB-mediated dislocation activity. Thus, the sharp change in the deformation behavior of nc HEA observed for T above 473 K can be attributed to the enhanced plasticity due to GB diffusion. It is noteworthy that although GB diffusion becomes more pronounced above 473 K, this nc HEA did not exhibit noticeable grain growth within the examined T range (see Fig. 3). It is known that for conventional nc Ni, appreciable grain growth occurs above 0.27T_m [38, 39]. Good thermal stability of nc HEAs has been often reported and rationalized by sluggish diffusion and/or the segregation-induced GB energy reduction [40, 41]. Since GB segregation is absent in the present nc HEA (Fig. 3), sluggish diffusion may play a crucial role in its excellent thermal stability.

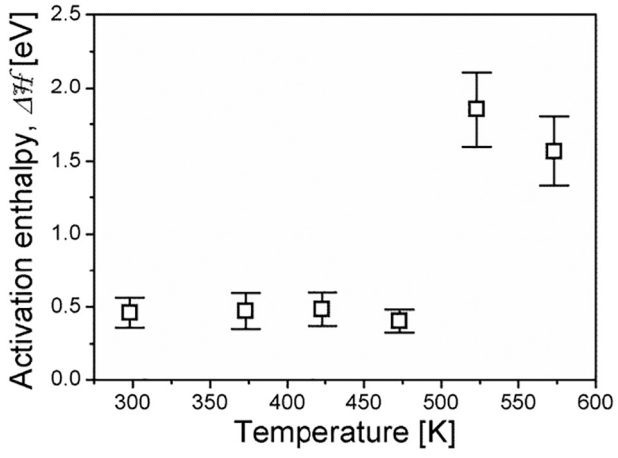

Fig. 4. Variations of the apparent activation enthalpy $\Delta\mathcal{H}$ of nc HEA with T.

In summary, the activation energy for the plastic flow of HPT-processed nc CoCrFeMnNi HEA was investigated through high-temperature nanoindentation experiments, results of which show that there is a sudden increase in the barrier from ~0.5 to ~1.8 eV at a T of 473 K. It was revealed that this increase is not caused by the microstructural instability but by the change in deformation mechanism, i.e., enhanced plasticity due to GB diffusion at high T.

The work at Hanyang University was supported by the National Research Foundation of Korea (NRF) grants funded by the Ministry of Science and ICT (No. 2015R1A5A1037627 and No. 2017R1A2B4012255). The work at Karlsruhe Institute of Technology was supported by the Deutsche Forschungsgemeinschaft DFG (German Research Foundation) under grant number SCHW 855/6-1 within the priority program SPP 2006 "Compositionally Complex Alloys - High Entropy Alloys (CCA-HEA)".

Appendix A. Supplementary data

Supplementary data to this article can be found online at https://doi.org/10.1016/j.scriptamat.2018.07.014.

References

[1] Y. Zhang, T.T. Zuo, Z. Tang, M.C. Gao, K.A. Dahmen, P.K. Liaw, Z.P. Lu, Prog. Mater. Sci. 61 (2014) 1–93.
[2] D.B. Miracle, O.N. Senkov, Acta Mater. 122 (2017) 448–511.
[3] Z. Wu, M.C. Troparevsky, Y.F. Gao, J.R. Morris, G.M. Stocks, H. Bei, Curr. Opin. Solid State Mater. Sci. 21 (2017) 267–284.
[4] Y. Zhao, D.-H. Lee, M.-Y. Seok, J.-A. Lee, M.P. Phaniraj, J.-Y. Suh, H.-Y. Ha, J.-Y. Kim, U. Ramamurty, J.-i. Jang, Scr. Mater. 135 (2017) 54–58.
[5] H. Gleiter, Prog. Mater. Sci. 33 (1989) 223–315.
[6] M.A. Meyer, A. Mishra, D.J. Benson, Prog. Mater. Sci. 51 (2006) 427–556.
[7] M. Dao, L. Lu, R.J. Asaro, J.T.M. De Hosson, E. Ma, Acta Mater. 55 (2007) 4041–4065.
[8] C.C. Koch, J. Mater. Res. 32 (2017) 3435–3444.
[9] B. Schuh, F.M. Martin, B. Völker, E.P. George, H. Clemens, R. Pippan, A. Hohenwarter, Acta Mater. 96 (2015) 258–268.
[10] D.-H. Lee, I.-C. Choi, M.-Y. Seok, J. He, Z. Lu, J.-Y. Suh, M. Kawasaki, T.G. Langdon, J.-i. Jang, J. Mater. Res. 30 (2015) 2804–2815.
[11] D.-H. Lee, M.-Y. Seok, Y. Zhao, I.-C. Choi, J. He, Z. Lu, J.-Y. Suh, U. Ramamurty, M. Kawasaki, T.G. Langdon, J.-i. Jang, Acta Mater. 109 (2016) 314–322.
[12] D.-H. Lee, J.-A. Lee, Y. Zhao, Z. Lu, J.-Y. Suh, J.-Y. Kim, U. Ramamurty, M. Kawasaki, T.G. Langdon, J.-i. Jang, Acta Mater. 140 (2017) 443–451.
[13] A. Heczel, M. Kawasaki, D. Ugi, J.-i. Jang, T.G. Langdon, J. Gubicza, Mater. Sci. Eng. A 721 (2018) 165–167.
[14] J.M. Wheeler, V. Maier, K. Durst, M. Göken, J. Michler, Mater. Sci. Eng. A 585 (2013) 108–113.
[15] V. Maier, C. Schunk, M. Göken, K. Durst, Philos. Mag. 95 (2015) 1766–1779.
[16] V. Maier-Kiener, B. Schuh, E.P. George, H. Clemens, A. Hohenwarter, J. Mater. Res. 32 (2017) 2658–2666.
[17] J.M. Wheeler, D.E.J. Armstrong, W. Heinz, R. Schwaiger, Curr. Opin. Solid State Mater. Sci. 19 (2015) 354–366.
[18] I.-C. Choi, C. Brandl, R. Schwaiger, Acta Mater. 140 (2017) 107–115.
[19] W.C. Oliver, G.M. Pharr, J. Mater. Res. 7 (1992) 1564–1583.
[20] O.D. Sherby, P.E. Armstrong, Metall. Trans. B 2 (1971) 3479–3484.
[21] A. Bolshakov, G.M. Pharr, J. Mater. Res. 13 (1998) 1049–1058.
[22] A. Barnoush, Acta Mater. 60 (2012) 1268–1277.
[23] K.L. Johnson, Contact Mechanics, Cambridge University Press, Cambridge, 1985.
[24] H. Conrad, Mater. Sci. Eng. A 341 (2003) 216–228.
[25] J.R. Trelewicz, C.A. Schuh, Scr. Mater. 61 (2009) 1056–1059.
[26] A.S. Argon, Strengthening Mechanisms in Crystal Plasticity, Oxford University Press, Oxford, 2008.
[27] Z. Wu, H. Bei, G.M. Pharr, E.P. George, Acta Mater. 81 (2014) 428–441.
[28] H.J. Frost, M.F. Ashby, Deformation-mechanism Maps: The Plasticity and Creep of Metals and Ceramics, Pergamon Press, Oxford, 1982.
[29] R.J. Asaro, S. Suresh, Acta Mater. 53 (2005) 3369–3382.
[30] P. Gu, M. Dao, R. Asaro, S. Suresh, Acta Mater. 59 (2011) 6861–6868.
[31] Y.M. Wang, A.V. Hamza, E. Ma, Acta Mater. 54 (2006) 2715–2726.
[32] Q. Lin, X. An, H. Liu, Q. Tang, P. Dai, X. Liao, J. Alloys Compd. 709 (2017) 802–807.
[33] M. Vaidya, K.G. Pradeep, B.S. Murty, G. Wilde, S.V. Divinski, Sci. Rep. 7 (2017) 12293.
[34] S.V. Divinski, G. Reglitz, H. Rösner, Y. Estrin, G. Wilde, Acta Mater. 59 (2011) 1947–1985.

[35] X. Sauvage, G. Wilde, S.V. Divinski, Z. Horita, R.Z. Valiev, Mater. Sci. Eng. A 540 (2012) 1–12.
[36] Z.W. Shan, E.A. Stach, J.M.K. Wiezorek, J.A. Knapp, D.M. Follstaedt, S.X. Mao, Science 305 (2004) 654–657.
[37] E. Ma, Science 305 (2004) 623–624.
[38] Y.M. Wang, S. Cheng, Q.M. Wei, E. Ma, T.G. Nieh, A. Hamza, Scr. Mater. 51 (2004) 1023–1028.
[39] T. Chookajorn, H.A. Murdoch, C.A. Schuh, Science 337 (2012) 951–954.
[40] S. Praveen, J. Basu, S. Kashyap, R. Kottada, J. Alloys Compd. 661 (2016) 361–367.
[41] N. Zhou, T. Hu, J. Huang, J. Luo, Scr. Mater. 124 (2016) 160–163.